Zero electron kinetic energy spectroscopy of the $ArCl^-$ anion

Thomas Lenzer,[a] Ivan Yourshaw,[b] Michael R. Furlanetto,[c] Georg Reiser,[d] and Daniel M. Neumark[e]
Department of Chemistry, University of California, Berkeley, California 94720, and Chemical Sciences Division, Lawrence Berkeley National Laboratory, Berkeley, California 94720

(Received 19 January 1999; accepted 23 February 1999)

Zero electron kinetic energy (ZEKE) spectroscopy has been utilized to study the $^{40}Ar^{35}Cl^-$ anion and the $X1/2$, $I3/2$ and $II1/2$ electronic states of neutral ArCl. Well-resolved progressions in the low-frequency vibrations of the anion and the neutral complexes are observed in the ZEKE spectra. From our spectroscopic data we construct model potential functions for the anion and three neutral states. This yields refined values for the neutral state splittings and the first accurate experimental $ArCl^-$ anion potential. Absolute uncertainties for R_m and ϵ in all potentials are estimated to be ± 0.08 Å and ± 0.6 meV, respectively. © *1999 American Institute of Physics.* [S0021-9606(99)01819-X]

I. INTRODUCTION

Over the last decades substantial experimental and theoretical effort has been directed toward the characterization of the potential energy function between weakly interacting species. Many key features governing the interaction between closed-shell neutral atoms and molecules are therefore now well understood.[1,2] However, information on the interactions between open- and closed-shell species is relatively scarce, and the same holds for the intermolecular forces between ions and neutrals. Infrared action spectroscopy has been utilized to investigate high frequency intramolecular vibrations in ion-neutral clusters,[3–6] but the region of low frequency vibrations characteristic of ion-neutral binding still remains largely unexplored.

In the domain of negatively charged species, anion zero electron kinetic energy (ZEKE) spectroscopy[7] has been very successful in characterizing such low-frequency vibrational modes in weak anion-neutral interactions. We have demonstrated this in several studies, in which we reported ZEKE spectra for selected diatomic[8–10] and polyatomic rare gas halide clusters (Rg_nX^-).[11,12] Here we extend our investigations to the $ArCl^-$ anion.

ZEKE spectroscopy of the RgX^- diatomics yields accurate anion and neutral two-body potentials. The anion potentials are needed as a reliable basis to assess quantitatively the structure, energetics and dynamics of larger halide clusters[11–13] as well as the importance of many-body effects in these and related species.[11,12] Charged Rg_nX^- clusters can be seen as the simplest model systems of microsolvation. Knowledge of the interactions between the ionic core and the surrounding solvent in these systems can provide valuable clues for the understanding of photophysical properties and reactivity of ions in solution, matrices, and crystals. RgX^- interaction potentials also have important practical applications, as they determine the transport properties of halide ions in rare gases, and are, for instance, needed to describe processes occurring in plasmas and discharges.

As far as the $ArCl^-$ anion is concerned, the only experimental information available so far is from ion mobility measurements.[14] In addition, three different *ab initio* calculations have been performed, one employing second-order many-body perturbation theory (MBPT2) with an extended basis set of approximate natural orbitals (ANOs),[15] another one utilizing second-order Møller–Plesset perturbation theory (MP2) and extended basis sets (with and without bond functions),[16] and the third one at the CCSD-T level of coupled cluster theory (aug-cc-pVQZ basis set).[17] These data are complemented by potentials deduced from several theoretical and (semi-)empirical models.[18–23] Additional experimental data as provided by our present ZEKE study are therefore highly desirable, especially as benchmarks for further theoretical studies.

The neutral RgX^1 complexes accessed by photodetachment of the anion are also of interest because of the open-shell nature of the halogen atom. Three molecular electronic states arise from the interaction between the ^2P halogen atom and the rare gas, as schematically shown for ArCl in Fig. 1.[24,25] The electrostatic interaction between the two atoms splits the lower $^2P_{3/2}$ state into two components arising from the two possible projections of the total electronic angular momentum Ω along the internuclear axis, $\Omega = 1/2$ (the $X1/2$ state or ''X'' state) and $\Omega = 3/2$ (the $I3/2$ or ''I'' state). The upper $^2P_{1/2}$ spin–orbit state of the atomic halogen correlates with another state in the complex, $II1/2$(''II''), characterized by $\Omega = 1/2$.

Much of the original interest in neutral RgX species originated from their use in excimer lasers, where lasing occurs through transitions between electronically excited, deeply bound charge transfer states (''Rg^+X^-'') and the re-

[a]DFG Postdoctoral Fellow. Present address: Institut für Physikalische Chemie, Universität Göttingen, Tammannstr. 6, 37077 Göttingen, Germany. Electronic mail: tlenzer@gwdg.de
[b]Present address: Aerodyne Research Inc., 45 Manning Road, Billerica, Massachusetts 01821-3976. Electronic mail: ivany@aerodyne.com
[c]NSF Predoctoral Fellow. Electronic mail: furl@radon.cchem.berkeley.edu
[d]Present address: Agfa, Abt. FT-EO, Tegernseer Landstr. 161, 81534 Munich, Germany.
[e]Electronic mail: dan@radon.cchem.berkeley.edu

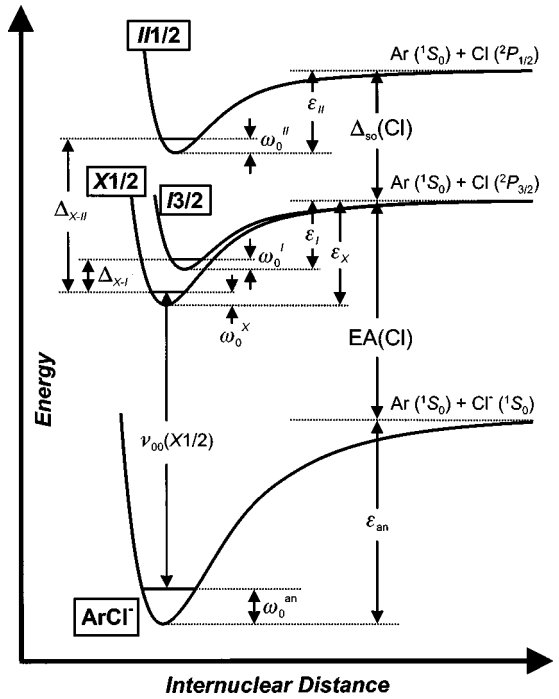

FIG. 1. Schematic diagram of potential energy levels involved in the photodetachment of the rare gas halide $ArCl^-$. The energetic relations among the atomic and molecular anion and neutral electronic states are shown. For a description of the various quantities see Sec. IV B.

pulsive wall of the weakly bound covalent ground states. The most widely known examples are XeCl, KrF, and ArF.

Early studies on ArCl include the observation of vacuum UV emission resulting from reactions of metastable argon atoms with Cl_2 and CCl_4.[26,27] These measurements, however, yielded only very limited information on the ArCl electronic states involved in this process. Very detailed information on the $X1/2$, $I3/2$, and $II1/2$ potential curves of ArCl came from absolute elastic total cross-section (TCS) measurements with magnetic selection of the chlorine atoms carried out by Aquilanti and co-workers.[25] More recently, coupled cluster calculations by Naumkin and McCourt[28] (CCSD-T with aug-cc-pVTZ and aug-cc-pVQZ basis sets) as well as Burcl *et al.*[29] [CCSD(T) with an aug-cc-pVTZ basis set including bond functions] yielded potential functions similar to Aquilanti's; but both predicted a larger $\Sigma-\Pi$ splitting which was outside the cited uncertainty limits of the scattering study. On the other hand, absolute total cross sections calculated on basis of the CCSD(T) potentials of Burcl *et al.* could not adequately describe the position and shape of the experimental ArCl glory structures. Additional experimentally determined potential functions for the different ArCl neutral states are therefore needed.

Our ZEKE experiments provide a comprehensive view of the $ArCl^{(-)}$ anion and neutral X, I, and II potentials. The ability to probe the anion is particularly important due to the absence of experimental spectroscopic information. Anion ZEKE spectroscopy is also particularly sensitive to the neutral state splittings, and this will allow us to show that, e.g., the $X-I$ splitting in ArCl is indeed larger than the one extracted from the scattering study.

The paper has been organized as follows: Sec. II provides a short overview of the setup used for the $ArCl^-$ ZEKE experiment. In Sec. III we present our experimental spectra and complete assignments of the observed transitions. Section IV focuses on the construction of model potentials for fitting the vibrational and rotational peak contours of the ZEKE spectra. A comparison of our potentials with the available literature data can be found in Sec. V. The precise potential functions obtained in this paper will be used in a forthcoming publication to elucidate the influence of many-body effects in larger $Ar_nCl^{(-)}$ clusters.[30]

II. EXPERIMENT

Detailed descriptions of the anion zero electron kinetic energy (ZEKE) spectrometer can be found elsewhere.[7,31–33] Here we focus on the specific details relevant to our study. $ArCl^-$ anions are generated by passing argon over CCl_4 (at 0 °C), which is then expanded into vacuum through a 0.5 mm aperture in a pulsed valve (General Valve Series 9), with a typical backing pressure of 60–100 psig.

The resulting free jet is crossed by a 1 keV electron beam. Negative ions are formed by dissociative attachment (and other secondary processes), and undergo clustering in the continuum flow region of the expansion. The anion cluster ions formed during these processes are cooled as the expansion progresses. They subsequently pass through a setup of two skimmers into a differentially pumped region. As in our Xe_nI^- studies,[10,12] the additional second skimmer in the source chamber appears to produce additional cooling, and we find a substantial enhancement in the yield of the larger clusters.

The clusters are then accelerated to 1 keV into a 1 m collinear time-of-flight mass spectrometer, where they separate according to their mass. After entering the detector region the $^{40}Ar^{35}Cl^-$ anions (subsequently denoted ''$ArCl^-$'') are photodetached by an excimer-pumped dye laser (Lambda Physik FL3002). As in our work on Xe_nI^- (Refs. 10, 12) a weak dc field of -15 mV/cm is applied across the electron detachment region at all times; this field, which is antiparallel to the ion beam propagation direction, slightly decelerates electrons in the laboratory frame.

After a delay of 400–500 ns the photodetached electrons are extracted collinearly by a weak pulsed field of 4 V/cm and deflected to an off-axis microchannel detector 1 m away from the extraction region. Temporal filtering is achieved by gating the electron detection. Moreover, an arrangement of apertures between the photodetachment point and the detector provides spatial discrimination. This combination of spatial and temporal filtering effectively discriminates against high energy electrons, so that as the laser wavelength is scanned, only threshold photoelectrons with almost zero kinetic energy are detected. Addition of the weak dc field is found to enhance the amount of ZEKE electrons by roughly a factor of 3, with no degradation of the spectral resolution of 1–2 cm^{-1} for atomic anions.[10] The peaks observed in this study are broader due to the unresolved rotational envelopes.

The experiment is operated at 30 Hz. For studying the X, I, and II states PTP dye (Exciton) is used with a typical energy of 3–30 mJ/pulse. The ZEKE spectra are normalized

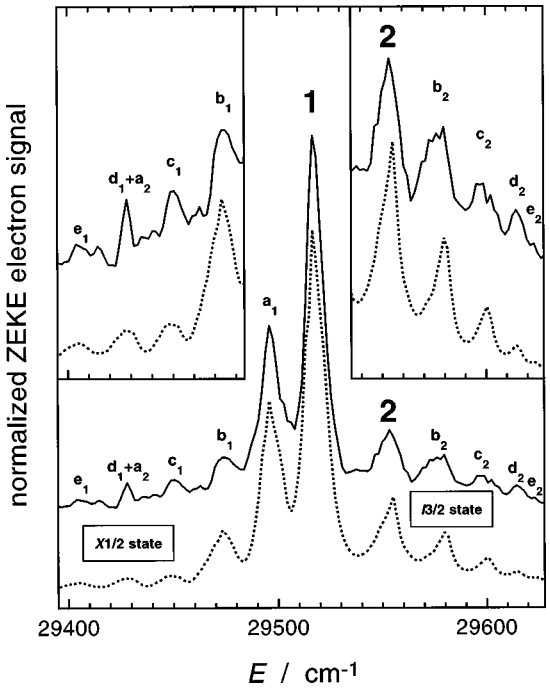

FIG. 2. Experimental and simulated $^{40}Ar^{35}Cl^-$ ZEKE spectra for the $X1/2$ and $I3/2$ states ($^2P_{3/2}$ asymptote). Solid lines, experimental data; dotted lines, best fit spectral simulation based on MSV model potentials, see text. Peaks **1** and a_1–e_1 are due to the X state and peaks **2** and a_2–e_2 belong to the I state; see Table I for complete assignments of all features. The two insets on the left and on the right show magnifications of the experimental and simulated spectra in the corresponding energy regions.

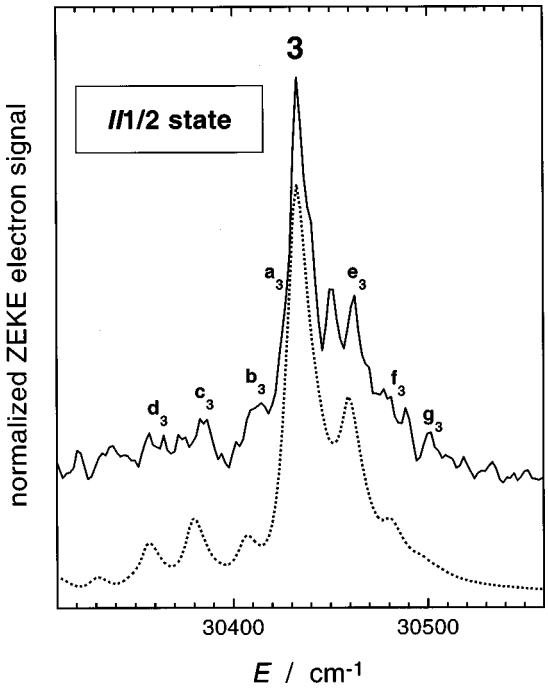

FIG. 3. Experimental and simulated $^{40}Ar^{35}Cl^-$ ZEKE spectra for the $II1/2$ state ($^2P_{1/2}$ asymptote). Solid line, experimental data; dotted line, best fit spectral simulation based on MSV model potentials, as described in text. For complete assignments of features **3** and a_3–g_3 see Table I.

to the ion signal and laser power, and averaged over 2000–4000 laser shots per point. Absolute vacuum wavelengths are obtained by calibration of the dye laser either with a New Focus 7711 Fizeau wavelength meter (X and I states) or a Fe/Ne hollow cathode lamp (II state).

III. ZEKE SPECTRA AND ASSIGNMENTS

As is already clear from the remarks in the introduction and Fig. 1, we expect to observe two band systems separated by approximately the spin–orbit constant of atomic chlorine ($882.4\,cm^{-1}=109.40\,meV$).[25] The lower energy band system is shown in Fig. 2, and results from transitions to the $X1/2$ and $I3/2$ states. The higher energy system in Fig. 3 is due to the $II1/2$ state. Spectral simulations (Sec. IV) are included in both figures as dotted lines, and a compilation of the assignments for all transitions are given in Table I.

The vibrational frequency of $ArCl^-$ is expected to be considerably larger than the frequencies for the three neutral ArCl states. Different types of neutral←anion transitions in the spectra can therefore be distinguished. First, there are vibrational progressions $v'-v''$ in which a series of neutral vibrational levels v' is populated by transitions originating from the anion ground vibrational state $v''=0$. Transitions of this type to neutral levels with $v'>0$ occur at higher energies than the 0–0 transition. There are also transitions originating from excited anion levels which can be further divided into sequence bands with *constant* Δv from a series of anion vibrational levels ($\Delta v=0$ and -1 are the most prominent observed in this study) and single hot band transitions ($\Delta v\neq 0$). These occur at lower energy than the 0–0 transition.

The spectrum in Fig. 2 is dominated by peak **1**, and a number of smaller peaks, denoted as a_1 to e_1, of decreasing

TABLE I. Peak assignments for the transitions between the $^{40}Ar^{35}Cl^-$ anion and the corresponding neutral $X1/2$, $I3/2$, and $II1/2$ states (Figs. 2 and 3). All energies are in cm^{-1}. The assignment listed first contributes the most to the peak intensity. Assignments in parentheses are additional transitions needed to account for at least two-thirds of the total peak intensity.

Peak	Position	Relative energy	v'(neutral)←v''(anion) assignment
1	29 516.7	0.0	0←0
a_1	29 495.9	−20.8	1←1
b_1	29 474.0	−42.7	2←2
c_1	29 450.0	−66.7	1←2 (3←3)
d_1	29 428.2	−88.5	2←3 (see also a_2)
e_1	29 405.0	−111.7	3←4 (1←3)
2	29 553.3	0.0	0←0
a_2	29 428.2	−125.1	1←3 (see also d_1)
b_2	29 576.2	+22.9	1←0
c_2	29 599.8	+46.5	2←0
d_2	29 614.6	+61.3	3←0
e_2	29 623.4	+70.1	4←0
3	30 432.9	0.0	0←0
a_3 (shoulder)	30 428.6	−4.3	2←1
b_3	30 412.7	−20.2	1←1
c_3	30 379.9	−53.0	0←1
d_3	30 360.6	−72.3	1←2
e_3	30 459.5	+26.6	1←0
f_3 (shoulder)	30 481.1	+48.2	2←0
g_3 (shoulder)	30 502.6	+69.7	3←0

intensity appear toward lower energy (see also the left inset in the same figure). We assign peak **1** to the origin (0–0) transition from the anion to the X state. The peaks a_1–c_1 are nearly equally spaced, by roughly 21 cm^{-1}, and are assigned to $\Delta v=0$ sequence band transitions from vibrationally excited anion states, i.e., the 1–1 to 3–3 transitions. Peak c_1 also shows a contribution from the 1–2 transition which together with peaks d_1 and e_1 (2–3 and 3–4) is part of the $(\Delta v=-1)$ sequence band with a characteristic spacing of about 22 cm^{-1}. The large intensity of the $X\leftarrow$anion 0–0 transition and the absence of v'-0 neutral progressions originating from the anion $v''=0$ level indicates that the equilibrium bond lengths of the anion and the X state are very similar, as seen in all our previous studies on RgX^- species.[8–10]

Spectral features in Fig. 2 above 29 540 cm^{-1} are due to $I3/2\leftarrow$anion transitions. In the upper right half of the figure, a second inset has been included, which shows a magnification of this part of the experimental spectrum and the corresponding spectral simulation. Peaks **2**, b_2...e_2 form a vibrational progression in the I state, with peak **2** assigned as the 0–0 transition and the latter four peaks as v'-0 transitions with $v'=1-4$ (spaced by roughly 23 cm^{-1}). The extent of this progression indicates that the bond length of the I state is significantly different from that of the anion, in apparent contrast to the X state. Moreover, the overall intensity of the I band is much lower than expected from the simulated Franck–Condon factors alone (only about 30% of the X state intensity as estimated from the spectral simulations). This is most likely due to different s-wave partial detachment cross sections near threshold for detachment to the X and I states, as was already observed in our study of XeI^-.[10]

The II state spectrum (Fig. 3) is dominated by peak **3** which we assign to the 0–0 transition. Additional assignments rely on the spectral simulation described below. The partially resolved peaks c_3 and d_3 left of the dip at about 30 400 cm^{-1} belong to the $\Delta v=-1$ sequence band (0–1, 1–2). Peak c_3 therefore yields an estimate for the anion vibrational frequency of about 53 cm^{-1}. The structure to the blue of the origin (peaks e_3–g_3) is due to a vibrational progression in the neutral ($v'-0$, with $v'=1-3$). The simulation shows that the additional peak between peaks **3** and e_3 must be due to experimental noise, as no other transitions can be present in this energy region. The resolution of the ZEKE spectrum for photodetachment to the $II1/2$ state is lower than for the X and I states, because the power of the dye laser fundamental in this wavelength region was much lower, and therefore the delay between photodetachment and electron extraction was slightly reduced to achieve acceptable signal rates. This results in a ZEKE linewidth of roughly 12 cm^{-1}, due to poorer discrimination against higher energy electrons. Nonetheless, some vibrational structure is seen.

IV. ANALYSIS

From peak **1** in Fig. 2 we directly obtain the accurate electron affinity of $29\,516.7\pm2.0\ cm^{-1}$ for $ArCl^-$. This value is larger than the corresponding electron affinity for atomic chlorine of 29 138.59 cm^{-1} (Ref. 34) and shows that the $ArCl^-$ dissociation energy is greater than that of ArCl, as expected. From the vibrational assignments in Table I we can also deduce frequencies for the anion and the three neutral states. For a more detailed description of the binding properties in the different ArCl species, it is necessary to construct flexible model potentials for the anion and neutral complexes from which the ZEKE spectra can be simulated. The potentials, fitting procedure, and results are described below.

A. Potential functions

We use a piecewise Morse-switching function-van der Waals (MSV) potential to fit our spectra. For neutral ArCl, the reduced form of this potential [with $f(x)=V(R)/\epsilon$ and $x=R/R_m$] is

$$\begin{aligned} f(x)&=e^{2\beta(1-x)}-2e^{\beta(1-x)}\equiv M(x), \quad 0<x\leqslant x_1,\\ &=SW(x)M(x)+[1-SW(x)]W(x), \quad x_1<x<x_2,\\ &=-C_{6r}x^{-6}-C_{8r}x^{-8}\equiv W(x), \quad x_2\leqslant x<\infty. \end{aligned} \tag{1}$$

Note that this form is different from our previous work, as we found it sufficient to use only a single Morse function (parameter β) to describe the well region and the repulsive wall, in contrast to the more elaborate MMSV function used earlier.[8–10,35] The switching function is calculated via

$$SW(x)=\frac{1}{2}\left[\cos\frac{\pi(x-x_1)}{(x_2-x_1)}+1\right], \tag{2}$$

and the reduced dispersion coefficients C_{nr} are given by

$$C_{6r}=\frac{C_6}{\epsilon R_m^6}, \quad C_{8r}=\frac{C_8}{\epsilon R_m^8}, \tag{3}$$

where ϵ is the potential well depth and R_m represents the equilibrium bond length (position of the potential minimum). C_6 is the induced dipole-induced dipole dispersion coefficient, and C_8 represents the corresponding coefficient for the induced dipole-induced quadrupole interaction. We adopt the same form for the $ArCl^-$ anion potential, the only exception being that the dispersion terms are replaced by

$$f(x)=-B_{4r}x^{-4}-B_{6r}x^{-6}\equiv W(x), \quad x_2\leqslant x<\infty, \tag{4}$$

with

$$B_{4r}=\frac{B_4}{\epsilon R_m^4}, \quad B_{6r}=\frac{B_6}{\epsilon R_m^6}, \tag{5}$$

and

$$B_4=\tfrac{1}{2}q^2\alpha_d(\mathrm{Ar}), \quad B_6=\tfrac{1}{2}q^2\alpha_q(\mathrm{Ar})+C_6. \tag{6}$$

Here, q is the chloride charge and B_4 represents the coefficient of the leading term in the long range $ArCl^-$ potential, reflecting the dipole induced in the argon atom by the chloride anion. B_6 is made up of quadrupole induction and dipole dispersion terms. α_d(Ar) and α_q(Ar) are the dipole and quadrupole polarizabilities of the argon atom, respectively, as given in Table II.

The dispersion coefficients C_6 and C_8 for the neutral ArCl $X1/2$, $I3/2$, and $II1/2$ states were estimated as prescribed in our earlier publication,[9] and the necessary parameters are also listed in Table II.[36–41] The C_6 parameter for the

TABLE II. Dipole and quadrupole polarizabilities and effective numbers of electrons used to calculate dispersion and induction coefficients for $ArCl^{(-)}$ interactions.

Atom	Corresponding spinless state of ArCl neutral	α_d (a_0^3)	α_q (a_0^5)	N
Cl	Σ	13.3[a]	73.2[b]	4.2[c]
	Π	15.3[a]	86.4[b]	4.2[c]
Ar	⋯	11.08[d]	52.78[e]	5.9[c]

[a]Reference 36; the spherically averaged value is $\alpha_d = 14.63$ a.u.
[b]Values from Ref. 37 rescaled by a factor of 0.8368: The spherically averaged α_q(Cl) from Ref. 37 is known to be too high so it was rescaled by a factor α_q(Ar, Ref. 38)/α_q(Ar, Ref. 37). This is slightly different from our prescription in Ref. 9, where α_q(Ar) from Ref. 41 instead of Ref. 38 was used for rescaling.
[c]Reference 40.
[d]Reference 39.
[e]Reference 38.

$ArCl^-$ anion was taken from *ab initio* calculations.[42] All C_6 and C_8 dispersion coefficients can be found together with the other potential parameters in Table III. The ZEKE spectra were not sensitive to the very long range part of the potential. Therefore B_4, B_6, C_6, and C_8 were not changed during the fitting procedure.

Unfortunately we cannot independently extract information on the equilibrium bond length for any of the potentials, because we are not able to resolve any rotational structure due to our limited experimental resolution ($\geqslant 1$ cm^{-1}). Similar problems occur for the well depth ϵ, because we are only sensitive to the differences between two electronic states. An external reference potential is therefore needed to determine the *absolute* position and well depth of one of our potential curves. The bond lengths and well depths of the remaining potentials can then be determined with high *relative* precision.

In our previous studies, ϵ and R_m for the $X1/2$ state were fixed based on either scattering or emission spectroscopy results. Here we use the position and well depth of the ArCl $I3/2$ state from Aquilanti's scattering study,[25] because this potential is also in very good agreement with the most recent CCSD(T) potential of Burcl *et al.*,[29] although ϵ is 0.3 meV less for the latter potential. The uncertainties in the reference values for ϵ and R_m are 0.6 meV and 0.08 Å, respectively. These values are considerably smaller than the uncertainties in the reference parameters used in our previous ZEKE studies,[8,9] with the exception of XeI^-, where additional information from ZEKE spectra of larger Xe_nI^- clusters allowed us to determine R_m with high precision.[10,12]

B. Fitting procedure

We used a discrete variable representation (DVR) procedure[43] based on a basis set of Morse potential eigenfunctions[44] to determine the vibrational eigenvalues and wave functions for the anion and neutral potentials. Once this was done, Franck–Condon factors were calculated, assuming a Boltzmann distribution for the population of the anion vibrational levels. These were used to produce a simulated vibrational stick spectrum. Finally, a set of rotational lines was calculated for each vibrational band, and these lines were convoluted with the ZEKE instrumental line shape to fit the observed asymmetric peak shapes; see Refs. 8 and 9 for more details.

The well depth of the $I3/2$ state potential was kept constant. Then the well depths for the remaining states were determined by using the following relationships implied by Fig. 1:

$$\epsilon_{an} = \nu_{00}(X1/2) + \omega_0^{an} + \epsilon_I - \omega_0^I + \Delta_{X-I} - \mathrm{EA(Cl)}, \tag{7}$$

$$\epsilon_X = \epsilon_I - \omega_0^I + \Delta_{X-I} + \omega_0^X, \tag{8}$$

$$\epsilon_{II} = \epsilon_X + \Delta_{\mathrm{so}}(\mathrm{Cl}) - \Delta_{X-II} - \omega_0^X + \omega_0^{II}. \tag{9}$$

$\nu_{00}(X1/2)$ represents the origin of the $X1/2$ state, $\omega_0^{an}, \omega_0^I$, etc. are zero point energies, EA(Cl) and Δ_{so}(Cl) are the electron affinity and the spin–orbit splitting of the chlorine atom, respectively. Δ_{X-I} is the $X1/2$–$I3/2$ state splitting (between the $v' = 0$ levels), and Δ_{X-II} denotes the $X1/2$–$II1/2$ state splitting.

TABLE III. MSV potential parameters and deduced spectroscopic constants for $^{40}Ar^{35}Cl$ and $^{40}Ar^{35}Cl^-$. Term values T_0 are referenced to the anion vibrational ground state. ω_0 = zero point energy, ν_{01} = fundamental vibrational frequency. Assumed anion temperature in the spectral simulations for $X1/2$,$I3/2$($II1/2$), $T_{\mathrm{vib}} = 110(120)$ K and $T_{\mathrm{rot}} = 80(60)$ K. Estimated fit uncertainties for potential parameters (±) given in parentheses.

	$X1/2$	$I3/2$	$II1/2$	Anion
T_0 (cm^{-1})	29 516.7 (2.0)	29 553.3 (2.0)	30 432.9 (3.0)	0
ω_0 (cm^{-1})	17.78	14.48	15.65	29.23
ν_{01} (cm^{-1})	31.86	25.23	27.16	53.09
ϵ (meV)[a]	16.77 (0.2, 0.6)	11.42 (0.2, 0.6)	12.10 (0.2,0.6)	64.87 (0.2, 0.6)
R_m (Å)[a]	3.73 (0.02, 0.08)	3.96 (0.02,0.08)	3.87 (0.02,0.08)	3.71 (0.02, 0.08)
β	6.21 (0.50)	6.57 (0.50)	6.73 (0.50)	5.30 (0.50)
x_1	1.000 (0.05)	1.050 (0.05)	1.110 (0.05)	1.025 (0.05)
x_2	2.660 (0.15)	1.454 (0.15)	1.582 (0.15)	1.260 (0.15)
C_6 (eV Å^6)	43.4 (6.5)	46.3 (7.0)	44.9 (6.7)	⋯
C_8 (eV Å^8)	308.3 (92.5)	333.6 (100.1)	320.9 (96.3)	⋯
B_4 (eV Å^4)	⋯	⋯	⋯	11.8 (1.8)
B_6 (eV Å^6)	⋯	⋯	⋯	98.1 (24.5)

[a]First number in parentheses is the uncertainty estimated from the fit of the ZEKE data, whereas the second number represents a possible absolute shift for all potentials (in the *same* direction) due to uncertainties in the $I3/2$ reference potential from scattering data (Ref. 25).

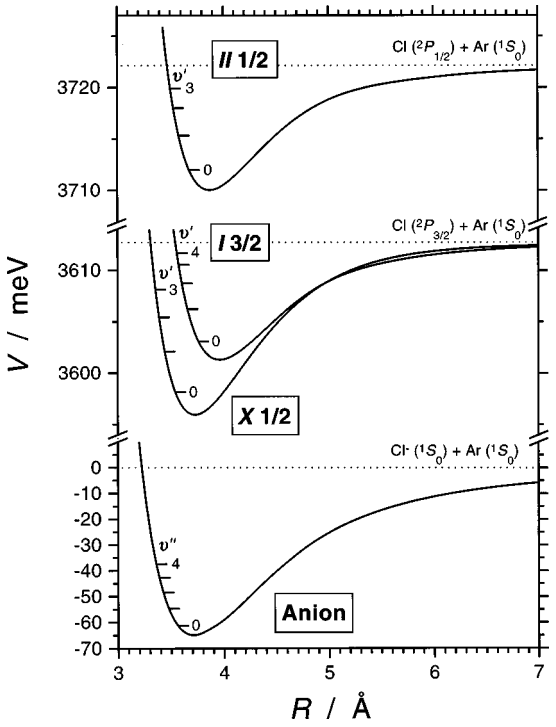

FIG. 4. Best fit MSV model potentials for the $ArCl^-$ anion and neutral $X1/2$, $I3/2$, and $II1/2$ states. Anion asymptote for $R\rightarrow\infty$ set to $E=0$, so the X and I states asymptotically converge toward the chlorine electron affinity [3612.726 meV (Ref. 34)] and the II state asymptote approaches the sum of the chlorine electron affinity and the chlorine spin–orbit splitting [Δ_{so}(Cl)=109.40 meV (Ref. 25)]. Note also the two breaks on the energy axis. Vibrational states involved in transitions (Table I) contributing to observed features in the spectra of Figs. 2 and 3 are marked by short dashes at the repulsive wall of each state.

Once all well depths were fixed, the potential parameters R_m, β, x_1, and x_2 of the anion, X, and II state potentials, the ZEKE linewidth, and the vibrational and rotational temperature of the anion were iteratively adjusted in a trial-and-error fashion to produce the best agreement between the experimental and simulated ZEKE spectra. From our spectral fits we deduced vibrational and rotational temperatures of $T_{\rm vib}=110(120)$ K and $T_{\rm rot}=80(60)$ K for the X and $I(II)$ states in good agreement with the results from our earlier studies of other RgX^- diatomics.[8–10] During the fitting procedure it was found necessary to increase the steepness of the $I3/2$ repulsive wall slightly (relative to the original shape of the TCS potential) to reproduce the vibrational spacings in the $I3/2$ state ZEKE spectrum (Fig. 2). The anion potential was constructed first to fit the $I3/2\leftarrow$anion band. Then, the potentials for the X and II states were determined by fitting their respective bands.

The present fits were subjected to the additional reasonable constraint that the three neutral potentials should yield an (almost) constant $\Delta_{so}(R)$.[24,45,46] The spin–orbit splitting for our best set of potential parameters obtained this way deviates by less than 1% relative to the value for atomic chlorine for all R values larger than the zero crossing point of the X state potential. A constant $\Delta_{so}(R)$ could not be reached without accepting a substantially worse fit quality.

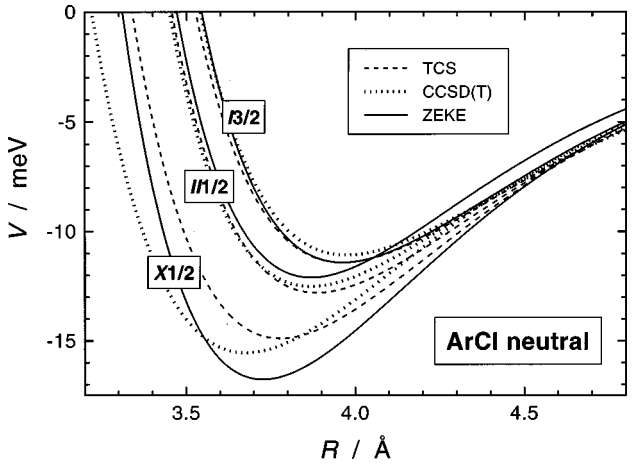

FIG. 5. Comparison of ArCl $X1/2$, $I3/2$, and $II1/2$ neutral potentials. Dashed lines, elastic TCS data from scattering experiments with magnetic selection of chlorine atoms (Ref. 25); dotted lines, CCSD(T) results from Ref. 29 (aug-cc-pVTZ basis set including bond functions); solid lines, anion ZEKE spectroscopy (this work). All potential curves are referred to the same asymptote. For characteristic potential quantities, see Table IV.

C. Best fit

The best fit potentials are shown in Fig. 4. Note that the energy scale in the plot for the X, I, and II states is magnified compared to the anion potential. The anion potential is about a factor of 4 deeper than the X state. For all potential curves the vibrational levels contributing to observed transitions in the spectra of Figs. 2 and 3 have been marked by short dashes on the side of the repulsive walls and numbered (compare Table I). The locations of the turning points corresponding to the highest energy levels contributing to spectral transitions allow us to estimate that the ZEKE $ArCl^{(-)}$ anion, X, I, and II state potentials should be well defined over the intervals $R=3.4$–4.6 Å, 3.4–4.9 Å, 3.6–6.1 Å, and 3.5–5.3 Å, respectively, corresponding to 42%, 73%, 91%, and 82% of the classical potential well depth.

Table III contains the best fit parameters of the potentials including estimated uncertainties. The corresponding spectral simulations have already been included in Figs. 2 and 3 as dotted lines and discussed in Sec. III. Because the parameters B_4 and B_6 (C_6 and C_8) for the anion (neutral) are established within $\pm15\%$ to $\pm30\%$ from either experimental or *ab initio* data (Sec. IV A), the behavior of our model potentials at large R should also be realistic. The $ArCl^-$ ZEKE spectra are however not sensitive to the higher energy region of the repulsive wall at short range. As in our previous studies, all the potentials can shift together within the uncertainties of the reference values used for R_m and ϵ; these are also tabulated in Table III.

V. DISCUSSION

A comparison of the ZEKE potentials for the ArCl neutral X, I, and II states with the scattering potentials from Ref. 25 and the *ab initio* potentials from Ref. 29 [CCSD(T) using an aug-cc-pVTZ basis set with bond functions] is shown in Fig. 5. Characteristic quantities are tabulated in Table IV. Note that we have not included the CCSD-T results of

TABLE IV. Comparison of equilibrium bond lengths R_m and well depths ϵ for ArCl neutral interactions from different studies.

		TCS[a]	CCSD(T)[b]	ZEKE
R_m (Å)	$X1/2$	3.78 (0.08)	3.68	3.73
	$I3/2$	3.96 (0.08)	3.97	3.96
	$II1/2$	3.89 (0.08)	3.87	3.87
ϵ (meV)	$X1/2$	14.9 (0.7)	15.5	16.8
	$I3/2$	11.4 (0.6)	11.1	11.4
	$II1/2$	12.8 (0.6)	12.5	12.1

[a]Reference 25 [cited uncertainties (±) are given in parentheses].
[b]*Ab initio* calculations from Ref. 29 using an aug-cc-pVTZ basis set with bond functions (values extracted from Tang–Toennies-type fits to the calculated points for the Σ and Π states).

TABLE V. Characteristic quantities of the ZEKE $ArCl^-$ anion potential compared to literature potentials.

Source	ϵ (meV)	R_m (Å)
Present work[a]	64.9 (0.6)	3.71 (0.08)
Ion mobilities[b]	103.7	3.14
Universal interaction potentials[c]	100.1	3.31
MBPT2cp (extended ANO basis set)[d]	58.8	3.73
CCSD-T (aug-cc-pVQZ basis set)[e]	59.1	3.71
Extended Tang–Toennies model[f]	64.2	3.75
Unified perturbative approach[g]	63.7	3.65
Polarizability correlations[h]	76	3.77
Modified polarizability correlations[i]	70	3.68
Modified electron gas theory[j]		
method I	92	3.39
method II	87	3.43
method III	79	3.49

[a]Uncertainties in R_m and ϵ estimated from the $I3/2$ state TCS reference potential of Ref. 25.
[b]Reference 14.
[c]Reference 22.
[d]Counterpoise corrected values from Ref. 15.
[e]BSSE corrected values from Ref. 17.
[f]References 20 and 21.
[g]Reference 19.
[h]Reference 23.
[i]As h, but using modified constants from Ref. 9.
[j]Reference 18.

Naumkin *et al.*[28] because their aug-cc-pVTZ and aug-cc-pQTZ basis sets appear to perform slightly worse than those of Burcl *et al.*[29]

All three sets of potentials exhibit the same well-known trends for the bond lengths and well depths as already observed in other RgX systems, namely $R_m(X)<R_m(II)<R_m(I)$ and $\epsilon(I)<\epsilon(II)<\epsilon(X)$. The X state has predominantly Σ character at short range. In this case the unpaired electron of the chlorine atom is directed along the Ar–Cl internuclear axis. In contrast, the I state is a pure Π state and the II state has predominantly Π character, i.e., the orientation of the unpaired electron is perpendicular to the internuclear axis. Aquilanti *et al.* explained the greater stabilization of the Σ state relative to the Π state in rare gas halogen systems by charge transfer due to configuration interaction between the lower lying neutral and higher lying ionic (Rg^+X^-) molecular states of the same symmetry.[25,47] On the other hand, the *ab initio* study by Burcl *et al.* indicates that minimization of exchange repulsion is the key factor for the stronger binding in the Σ state of ArCl (and also NeCl and HeCl).[29]

For the I state, as mentioned above, our values for R_m and ϵ were fixed at Aquilanti's values. Table IV and Fig. 5 show that our II state is slightly shallower than the TCS and CCSD(T) potentials, but R_m is essentially identical for all three potentials. More substantial differences are found for the $X1/2$ state, where our ZEKE study yields a deeper well than the TCS and CCSD(T) potentials. Aquilanti's data result in a $X-I$ splitting of 25.9 cm^{-1} (including zero point energies) whereas from the spacing of peaks **1** and **2** in the ZEKE spectrum of Fig. 2 one directly obtains 36.6 cm^{-1} (Table I). Note that the splitting we obtain is independent of the choice of the reference potential. It therefore appears that the scattering study underestimates the $\Sigma-\Pi$ splitting.

Our conclusion that Aquilanti's X state potential is too shallow results from our choice of Aquilanti's $I3/2$ potential as the reference. There is additional if somewhat indirect evidence that suggests this conclusion is correct. A comparison between recent differential scattering cross-section data for the $ArCl_2$ complex[48] and theoretical $ArCl_2$ results[28] obtained from a model based on Aquilanti's diatomic ArCl potentials shows that the calculations underestimate the experimental well depth for the linear Ar···Cl–Cl configuration, which is mainly influenced by the ArCl Σ state potential. In contrast, for the T-shaped $ArCl_2$ configuration, where the interaction is dominated by the ArCl Π state, good agreement between the theoretical model and experiment is found.

Concluding the remarks on the ArCl X state potential, we find its bond length to be 0.05 Å shorter than Aquilanti's, though 0.05 Å larger than in the coupled cluster calculations of Ref. 29. Note also that the lower part of the repulsive wall of the ZEKE X state potential is somewhat steeper than both the TCS and CCSD(T) potentials (Fig. 5).

We now consider the $ArCl^-$ anion potential obtained from our ZEKE experiments. The anion well depth is four to six times larger than that of the neutral states because of the much stronger attraction due to the leading charge-induced dipole term and the additional charge-induced quadrupole contribution [Eq. (5)]. R_m is slightly increased upon photodetachment to the X state by +0.02 Å (Table III). The similarity of the bond length for the anion and X states is characteristic for all rare gas halide pairs studied so far, although in most cases a very slight shortening of R_m upon photodetachment was observed.[8–10,12] For comparison with previous studies of the $ArCl^-$ system, we have summarized available R_m and ϵ data in Table V. Selected potential curves from different sources are compared in Fig. 6.

The only other experimental information comes from ion mobility data,[14] which yield a substantially larger well depth and a considerably shorter equilibrium bond length, far outside the uncertainty limits of the ZEKE data. Large deviations of the same sign and magnitude between ZEKE potentials and ion mobility data were also found for all other systems studied so far.[8–10,12,49] This seems to point toward systematic errors in the ion mobility data inversion procedure. Note that the values predicted by the ''universal interaction potential model'' [22] in Table V likely suffer from the

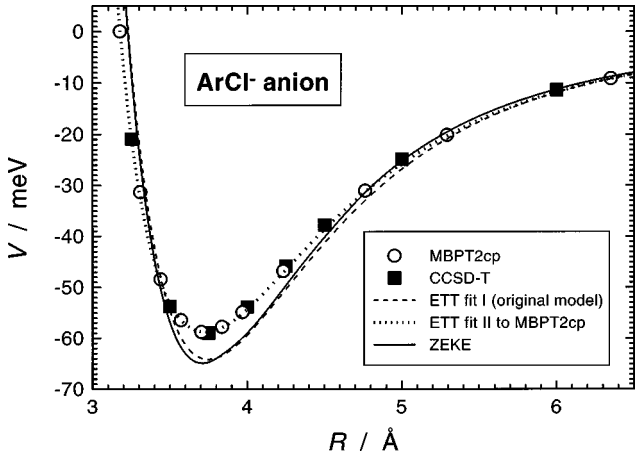

FIG. 6. Comparison of $ArCl^-$ anion potentials. ○, counterpoise corrected MBPT2 points from Ref. 15 (extended ANO basis set); ■, BSSE corrected CCSD-T points from Ref. 17 (aug-cc-pVQZ basis set); dashed line, original ''Extended Tang–Toennies (ETT) model'' from Refs. 20 and 21; dotted line, fit to MBPT2 points on basis of the modified ETT model (Refs. 50 and 51); solid line, anion ZEKE spectroscopy (this work). For characteristic potential quantities see Table V.

same problems as their short-range part is also based on the ion mobility data.

Three different *ab initio* calculations are available in the case of $ArCl^-$; The MBPT2 (Ref. 15) and CCSD-T (Ref. 17) studies (using extended ANO and aug-cc-pVQZ basis sets, respectively) yield very similar results (Fig. 6), and are also in agreement with a single-point MP2 calculation (employing an extended basis set with bond functions) for the minimum of the anion well.[16] They are very close to the ZEKE results for R_m but predict a somewhat smaller ϵ (Table V). If additional uncertainties introduced by the necessary correction for basis set superposition errors are kept in mind, both calculations appear to be in very good agreement with the ZEKE potential.

Several models to predict ion-neutral interactions have been published. We found the ''Extended Tang–Toennies model (ETT)'' by Ahlrichs *et al.*[20,21] to perform exceptionally well, as it shows almost complete agreement with the ZEKE potential (Fig. 6). A recently introduced modification of the ETT model[50,51] based on parameters of the MBPT2 calculations from Ref. 15 yields essentially the same potential as the *ab initio* study.

Patil's ''unified perturbative approach''[19] is in good agreement with the ZEKE results, though the R_m extracted from that model might be slightly too short (Table V). The results of Cappelletti *et al.* were obtained by very simple formulas based on empirically determined polarizability correlations.[23] Their results for R_m and ϵ both exceed our values. In a very recent publication we used our ZEKE data on several other RgX diatomics[8,9] for a recalibration of the numerical coefficients in their correlation formulas. When using these values the agreement is improved. Finally, all variations of the ''modified electron gas theory'' of Kim and Gordon result in a much higher well depth but a substantially shorter equilibrium bond length than our data indicate.[18]

VI. CONCLUSIONS

ZEKE spectroscopy of the $^{40}Ar^{35}Cl^-$ anion was used to characterize the anion and neutral potentials involved in the photodetachment of this diatomic rare gas halide cluster. A simulation of the ZEKE spectra for the $X1/2$, $I3/2$, and $II1/2$ states accessed by the photodetachment process allowed an assignment of all features in the spectra. We extracted model potentials for the anion, $X1/2$, $I3/2$, and $II1/2$ states involved, which defined the *relative* positions and shapes of all electronic states in the Franck–Condon region with high accuracy.

External experimental information on one of the four potential curves was necessary to pinpoint the *absolute* position of all potentials. For this purpose we used Aquilanti's $I3/2$ state potential from elastic total cross-section measurements with magnetic state selection of the chlorine atom.[25] Due to the precision of this potential and its good agreement with results from coupled cluster calculations[29] we estimate the uncertainties of all our potentials to be about ± 0.08 Å (R_m) and ± 0.6 meV (ϵ).

The ZEKE data are fully consistent with the *I* and *II* state potentials from the scattering and *ab initio* studies. However, our analysis yielded a deeper *X* state potential well which suggests that the scattering study slightly underestimated the Σ–Π splitting. We obtain the first accurate experimental potential for the $ArCl^-$ anion, which is in good agreement with *ab initio* results and several model potentials but not with the potential from ion mobility data.

Characteristic quantities like the equilibrium bond length R_m and well depth ϵ for all our $ArCl^{(-)}$ anion and neutral potentials are consistent with trends observed in our previous ZEKE studies of other rare gas halides.[8–10] In the ZEKE spectra, we found the intensity of the *I* state relative to the *X* state to be smaller than expected. As in our earlier study of XeI^- this is probably due to pronounced differences in the *s*-wave partial detachment cross sections to both states.[10]

Very recently, we have also obtained results for larger Ar_nCl^- clusters up to $n=15$. The analysis of this data on basis of the diatomic potentials obtained from the current study will be presented in a forthcoming publication to assess the importance of nonadditive effects in these polyatomic complexes.[30]

ACKNOWLEDGMENTS

This research is supported by the Air Force Office of Scientific Research under Grant No. F49620-97-1-0018. T. Lenzer is grateful to the Deutsche Forschungsgemeinschaft for a postdoctoral fellowship, and M. R. Furlanetto thanks the National Science Foundation for a predoctoral fellowship. We thank F. Y. Naumkin and F. R. W. McCourt for useful discussions and making the calculated $ArCl^{(-)}$ potentials of Refs. 17 and 28 available prior to publication. We also thank G. Chałasinski for a preprint of Ref. 29.

[1] R. A. Aziz, in *Inert Gases*, edited by M. L. Klein (Springer, Berlin, 1984), p. 5.
[2] G. Chałasinski and M. M. Szczesniak, Chem. Rev. **94**, 1723 (1994).
[3] J.-H. Choi, K. T. Kuwata, Y.-B. Cao, and M. Okumura, J. Phys. Chem. A **102**, 503 (1998).

[4] P. Ayotte, C. G. Bailey, G. H. Weddle, and M. A. Johnson, J. Phys. Chem. A **102**, 3067 (1998).
[5] J. M. Lisy, Int. Rev. Phys. Chem. **16**, 267 (1997).
[6] H. Linnartz, T. Speck, and J. P. Maier, Chem. Phys. Lett. **288**, 504 (1998).
[7] T. N. Kitsopoulos, I. M. Waller, J. G. Loeser, and D. M. Neumark, Chem. Phys. Lett. **159**, 300 (1989).
[8] Y. Zhao, I. Yourshaw, G. Reiser, C. C. Arnold, and D. M. Neumark, J. Chem. Phys. **101**, 6538 (1994).
[9] I. Yourshaw, T. Lenzer, G. Reiser, and D. M. Neumark, J. Chem. Phys. **109**, 5247 (1998).
[10] T. Lenzer, M. R. Furlanetto, K. R. Asmis, and D. M. Neumark, J. Chem. Phys. **109**, 10754 (1998).
[11] I. Yourshaw, Y. Zhao, and D. M. Neumark, J. Chem. Phys. **105**, 351 (1996).
[12] T. Lenzer, M. R. Furlanetto, N. Pivonka, and D. M. Neumark, J. Chem. Phys. (in press).
[13] Y. Zeiri, J. Phys. Chem. A **102**, 2785 (1998).
[14] C. C. Kirkpatrick and L. Viehland, Chem. Phys. **98**, 221 (1985).
[15] V. Kellö and A. J. Sadlej, Chem. Phys. **157**, 123 (1991).
[16] R. Burcl, S. M. Cybulski, M. M. Szczesniak, and G. Chałasinski, J. Chem. Phys. **103**, 299 (1995).
[17] F. Y. Naumkin and F. R. W. McCourt, Chem. Phys. Lett. **292**, 63 (1998).
[18] Y. S. Kim and R. G. Gordon, J. Chem. Phys. **61**, 1 (1974).
[19] S. H. Patil, J. Chem. Phys. **89**, 6357 (1988).
[20] R. Ahlrichs, H. J. Böhm, S. Brode, K. T. Tang, and J. P. Toennies, J. Chem. Phys. **88**, 6290 (1988).
[21] R. Ahlrichs, H. J. Böhm, S. Brode, K. T. Tang, and J. P. Toennies, J. Chem. Phys. **98**, 3579 (1993).
[22] A. D. Koutselos, E. A. Mason, and L. A. Viehland, J. Chem. Phys. **93**, 7125 (1990).
[23] D. Cappelletti, G. Liuti, and F. Pirani, Chem. Phys. Lett. **183**, 297 (1991).
[24] H. Haberland, Z. Phys. A **307**, 35 (1982).
[25] V. Aquilanti, D. Cappelletti, V. Lorent, E. Luzzatti, and F. Pirani, J. Phys. Chem. **97**, 2063 (1993).
[26] M. F. Golde and B. A. Thrush, Chem. Phys. Lett. **29**, 486 (1974).
[27] M. F. Golde, J. Mol. Spectrosc. **58**, 261 (1975).
[28] F. Y. Naumkin and F. R. W. McCourt, J. Chem. Phys. **107**, 5702 (1997).
[29] R. Burcl, R. V. Krems, A. A. Buchachenko, M. M. Szczesniak, G. Chałasinski, and S. M. Cybulski, J. Chem. Phys. **109**, 2144 (1998).
[30] T. Lenzer, I. Yourshaw, M. R. Furlanetto, and D. M. Neumark, J. Chem. Phys. (to be published).
[31] C. C. Arnold, Y. Zhao, T. N. Kitsopoulos, and D. M. Neumark, J. Chem. Phys. **97**, 6121 (1992).
[32] T. N. Kitsopoulos, Ph.D. thesis, University of California, Berkeley, 1991.
[33] C. C. Arnold, Ph.D. thesis, University of California, Berkeley, 1994.
[34] U. Berzinsh, M. Gustafsson, D. Hanstorp, A. Klinkmüller, U. Ljungblad, and A.-M. Martensson-Pendrill, Phys. Rev. A **51**, 231 (1995).
[35] P. Casavecchia, G. He, R. K. Sparks, and Y. T. Lee, J. Chem. Phys. **77**, 1878 (1982).
[36] K. Andersson and A. J. Sadlej, Phys. Rev. A **46**, 2356 (1992).
[37] L. J. Bartolotti, L. Ortiz, and Q. Xie, Int. J. Quantum Chem. **49**, 449 (1994).
[38] C. Hättig and B. A. Hess, J. Phys. Chem. **100**, 6243 (1996).
[39] A. Kumar and W. J. Meath, Mol. Phys. **54**, 823 (1985).
[40] E. A. Mason and E. W. McDaniel, *Transport Properties of Ions in Gases* (Wiley, New York, 1988).
[41] A. J. Thakkar, H. Hettema, and P. E. S. Wormer, J. Chem. Phys. **97**, 3252 (1992).
[42] C. Hättig and B. A. Hess, J. Chem. Phys. **108**, 3863 (1998).
[43] J. C. Light, I. P. Hamilton, and J. V. Lill, J. Chem. Phys. **82**, 1400 (1985).
[44] E. M. Greenawalt and A. S. Dickinson, J. Mol. Spectrosc. **30**, 427 (1969).
[45] V. Aquilanti, G. Liuti, F. Pirani, and F. Vecchiocattivi, J. Chem. Soc., Faraday Trans. 2 **85**, 955 (1989).
[46] V. Aquilanti and G. Grossi, J. Chem. Phys. **73**, 1165 (1980).
[47] V. Aquilanti, D. Cappelletti, and F. Pirani, Chem. Phys. Lett. **271**, 216 (1997).
[48] A. Rohrbacher, K. C. Janda, L. Beneventi, P. Casavecchia, and G. G. Volpi, J. Phys. Chem. A **101**, 6528 (1997).
[49] L. A. Viehland and C. C. Kirkpatrick, Chem. Phys. **202**, 285 (1996).
[50] E. J. Mansky and M. R. Flannery, J. Chem. Phys. **99**, 1962 (1993).
[51] E. J. Mansky and M. R. Flannery, J. Chem. Phys. **100**, 5391 (1994).